

Article

Application of Femtosecond Laser Processing Method in the Sustainable Conservation of Stone Cultural Relics: An Example of Green Schist in Wudang Mountain, China

Mu Chen ¹, Chengaonan Wang ^{1,*}, Kai Li ², Xianshi Jia ² , Cong Wang ² and Yansong Wang ^{1,*}¹ School of Urban Design, Wuhan University, Wuhan 430072, China; chenmu_1985@126.com² State Key Laboratory of Precision Manufacturing for Extreme Service Performance, College of Mechanical and Electrical Engineering, Central South University, Changsha 410083, China; likai01@csu.edu.cn (K.L.); 221026@csu.edu.cn (X.J.); wangcong@csu.edu.cn (C.W.)

* Correspondence: wcn1818@126.com (C.W.); 00011853@whu.edu.cn (Y.W.)

Abstract: The ancient building complex in Wudang Mountain, China, is known as the “Museum of Ancient Chinese Architectural Accomplishments”. However, the valuable stone components are preserved in open or semi-open environments and environmental factors such as rain seriously threaten its sustainable conservation. In this context, a femtosecond laser processing method has been demonstrated to be able to prepare hierarchical micro-nano structures on the stone surface to regulate its wettability, achieving the purpose of sustainable conservation. In this paper, the processing mechanism and performance of the femtosecond laser on green schist, a local stone material in the Wudang Mountain, are systematically investigated. It is found that green schist, as a typical non-homogeneous material, exhibits significant differences in its absorption of femtosecond laser with different compositions. Among them, quartz, chlorite, and muscovite are the three main compositions, and they are mainly characterized by cold ablation, thermal melting, and expansion under the irradiation of the femtosecond laser (238 fs, 100 kHz, 40 μJ, 33 μm, 500–40,000 pulses), respectively, and it is difficult to achieve a uniform and stable surface structure. Based on this, we prepared grooves with a spacing of 100–400 μm by scanning the femtosecond laser. Through the characterization of surface morphology, elemental composition, and three-dimensional structure, the processing mechanism of the hierarchical micro-nano structures of green schist under the irradiation of the femtosecond laser is comprehensively revealed. Finally, the wettability modulation result of water contact angle up to 147° is achieved by processing the grooves with an optimal spacing of 400 μm. The results of this research are of guiding significance for the sustainable conservation of ancient buildings and cultural relics.

Keywords: sustainable conservation; Wudang Mountain; femtosecond laser; superwetting surface; water contact angle



Citation: Chen, M.; Wang, C.; Li, K.; Jia, X.; Wang, C.; Wang, Y. Application of Femtosecond Laser Processing Method in the Sustainable Conservation of Stone Cultural Relics: An Example of Green Schist in Wudang Mountain, China. *Sustainability* **2024**, *16*, 3169. <https://doi.org/10.3390/su16083169>

Academic Editors: Francesca Di Turo and Giacomo Fiocco

Received: 28 February 2024

Revised: 29 March 2024

Accepted: 7 April 2024

Published: 10 April 2024



Copyright: © 2024 by the authors. Licensee MDPI, Basel, Switzerland. This article is an open access article distributed under the terms and conditions of the Creative Commons Attribution (CC BY) license (<https://creativecommons.org/licenses/by/4.0/>).

1. Introduction

The ancient building complex in Wudang Mountain, China, known as the “Museum of Ancient Chinese Architectural Accomplishments”, represents the pinnacle of artistic achievements in China, spanning a millennium. The stone components in the Wudang Mountain, such as stone pillars, beams, and Sumeru Seats, have both functional and symbolic significances, showcasing exceptional skill and artistic value in prehistoric China stonework [1,2]. However, these historic stone components, mostly preserved in open or semi-open environments and affected by rain and other environmental factors, are now showing varying degrees of deterioration, which has compromised the historical value of cultural relics [3]. Therefore, how to scientifically and sustainably conserve the stone components in Wudang Mountain has become a new challenge.

A common approach to the sustainable conservation of stone components is to prepare water repellents on the material surface to minimize the physical or chemical reaction of acidic or alkaline water acting on the substrate by controlling the contact between the material surface and water [4,5]. To achieve hydrophobicity, it is necessary to reduce the free energy of the material surface while also increasing the roughness of the material surface [6]. In this context, polymeric resins are commonly used as hydrophobic coatings for stone component conservation. The micro-nano structures of plants with hydrophobic properties in nature are often used as a reference, and close structures can be achieved by brushing or spraying a polymeric resin coating to create a micro- and nano-hierarchical roughness, thus obtaining hydrophobic properties [7,8]. However, the water repellents adopted usually contain ingredients that are hazardous to humans or the environment or alter the structure of the stone component itself and are not yet a widely adopted method [9]. Therefore, environmentally friendly hydrophobic structures have become of new interest. For example, by adding the non-toxic lauric acid into the substrate to reduce the surface energy and then covering stainless steel mesh to obtain rough hierarchical structures, a superhydrophobic surface exhibited water contact angle (WCA) of 153° could be obtained [10]. Alternatively, sand modified with stearic acid to provide low surface energy and sandpaper polishing to provide a superhydrophobic rough structure could result in a superhydrophobic WCA of 154° too [11]. These novel approaches can enhance the hydrophobic properties of materials, but they all require the addition of new coatings to the surface of stone components, which is not usually an appropriate option for the sustainable conservation of cultural relics.

In recent years, superwetting surfaces, i.e., superhydrophobic/superhydrophilic surfaces, have received tremendous attention from researchers [12–14]. Up to now, a number of methods have been developed for the fabrication of superwetting surfaces, including coating [15,16], templating [17], electrospinning [18], etching [19], and laser processing [20,21]. Among many methods, laser processing has become a research hotspot for the preparation of superwetting surfaces due to its high precision, non-contact, and environmentally friendly properties [22]. At present, the laser processing method has been widely used to prepare hydrophobic structures on a variety of material surfaces, such as metals [23], ceramics [24], glass [25], etc., while laser processing of hydrophobic structures on stone material surfaces is still in its infancy. In this regard, to the best of our knowledge, the earliest study was reported in 2017 by A. Chantada et al. The possibility of preparing hydrophobic structures on the surface of Zimbabwe black granites by nanosecond laser was explored. Zimbabwe black granites are principally composed of quartz, calcium-rich plagioclase feldspar, and orthopyroxenes, containing also small proportions of biotite and diopsides. Different absorption of laser by different compositions led to rougher surfaces, which reduced the WCA, and thus, made it difficult to develop effective hydrophobic properties. However, it was found that the hydrophobicity of the surface was enhanced at a low roughness due to the formation of smaller micro- and nanostructures constituting air pockets (the water is not able to penetrate the grooves owing to the surface tension of the droplet, leaving them full of air). Ultimately, the WCA could be increased by 45% using a 532 nm nanosecond laser (from 58° to 84°) [26]. In addition, an organically modified silica coating to reduce surface energy before the nanosecond laser processing proved to further enhance the hydrophobic properties [27].

In terms of laser-matter interactions, the ultrafast laser-matter interaction usually reflects smaller thermal effects, especially for some non-metallic materials (e.g., quartz composition in the stone materials). Ultrafast lasers are also able to form selective cold ablations, which allow for an overall higher processing quality [28]. In this context, the ultrafast laser processing method is also an alternative use in the preparation of superwetting structures on stone material surfaces [29–31]. As early as 2019, Ana J. López et al. [30] processed structures, such as grooves and holes, by femtosecond laser on the marble (Crystal White) surface and explored the corresponding wettability. Unlike previous studies, this marble contains high-purity calcite, which embodies a uniformly white,

equigranular structure, thus allowing the formation of stable micro-nano structures by the processing of the femtosecond laser. As a result, after exploring different femtosecond laser processing parameters, the WCA of the marble surface was increased from 66° to 134° , and in some cases, even the contact angle values close to superhydrophobic behavior were obtained. This work realized the transition from hydrophilic to hydrophobic behavior of the marble surface and explained the mechanism, considering the Cassie–Baxter model of wettability. It is also suggested that the ultrafast laser prepared air pockets between the marble surface and water droplets by processing a hierarchical structure, thus realizing hydrophobic behavior [30]. Drawing on the superhydrophobic structure on the surface of a lotus leaf, in 2022, Rocío Ariza et al. [31] processed similar micro-nano structures on the marble surface by grooving with a femtosecond laser. A femtosecond laser with a repetition rate of 500 kHz was adopted to maximize the nonlinear absorption and heat accumulation effects. In this context, a hierarchical structure formed by grooves with different spacing (micro-roughness, tens of micrometer depths) and covered by a flake-like morphology (nano-roughness) was processed on the marble surface, belonging to the typical hierarchical micro-nano structures. Meanwhile, the interesting result of increasing hydrophobicity of the marble surface with time (close to 300 days) was observed, although the sample surface presented hydrophilic properties after the femtosecond laser processing. It was concluded that the laser processing triggered two different effects: an “initialization” of the chemical state of the surface that turns much more reactive (likely because of the thermal decomposition of CaCO_3 at the near-surface of the laser-treated region) and an increase in the surface-to-volume ratio, favoring the extent of incorporation of water (hydroxylation) and (likely) C-H contaminants. Eventually, the WCA was able to stabilize at approximately 140° after close to 8–11 months [31].

However, in the case of natural stones used for the stone components, as is the case with the green schist mostly used in the Wudang Mountains, they are typically non-homogeneous materials. In the femtosecond laser processing of micro-nano structures, it is more common that the mechanisms of the interaction of the femtosecond laser to different grains are different, thus creating non-homogeneous surface structures through irregular surface absorption. Taking this into account, Ana J. López et al. [29] explored the wettability embodied by the femtosecond laser processing of four different materials (slate, quartzite, granite, and marble) and found that only the compositionally stabilized marble embodied a certain amount of hydrophobic properties. For the other three materials, due to the heterogeneity nature of the materials, irregular patterns were formed, affecting the hydrophobic properties of the material surfaces. These irregularities were measured on scales much larger than micrometers, which affected the continuity and periodicity of the laser-processed patterns, and thus the potential effect that this treatment may have on material wettability [29]. Recently, the structural characteristics of different stone compositions processed by femtosecond laser ablation have been further analyzed [32]. It can be found that some researchers have already explored the different responses of non-homogeneous stone materials to ultrafast laser irradiation from the perspective of laser-matter interaction and tried to apply them in the wettability regulation.

In this paper, taking green schist, a non-homogeneous stone material from Wudang Mountain, as an example, we systematically investigated the surface characteristics and processing mechanisms of different material compositions of green schist. Based on this, the differences in the micro-nano structures and corresponding wettability properties formed under different femtosecond laser parameters are explored, and ultimately, a superhydrophobic result was achieved.

2. Materials and Methods

2.1. Materials

The stone components of the ancient building complex in Wudang Mountain are mostly constructed of green schist [3]. In these experiments (Figure 1), the green schist samples with a size of $30\text{ mm} \times 30\text{ mm} \times 6\text{ mm}$ were formed by wire electrical discharge

machining (WEDM) cutting large green schist with a line-cut spacing of 1.5 mm (Figure 1b). Therefore, millimeter-width textures were formed on the surface of the initial samples. As examined by plane and cross-polarized light microscopy, the green schist (transverse) samples were found to consist of quartz, chlorite, muscovite, black mica, carbonate, and a small amount of dusty carbonaceous material. The three main compositions are 40% quartz, 35% chlorite, and 15% muscovite. The sample has a complex composition and is a typical non-homogeneous material, the WCA of the untreated sample is 42° (Figure 1b).

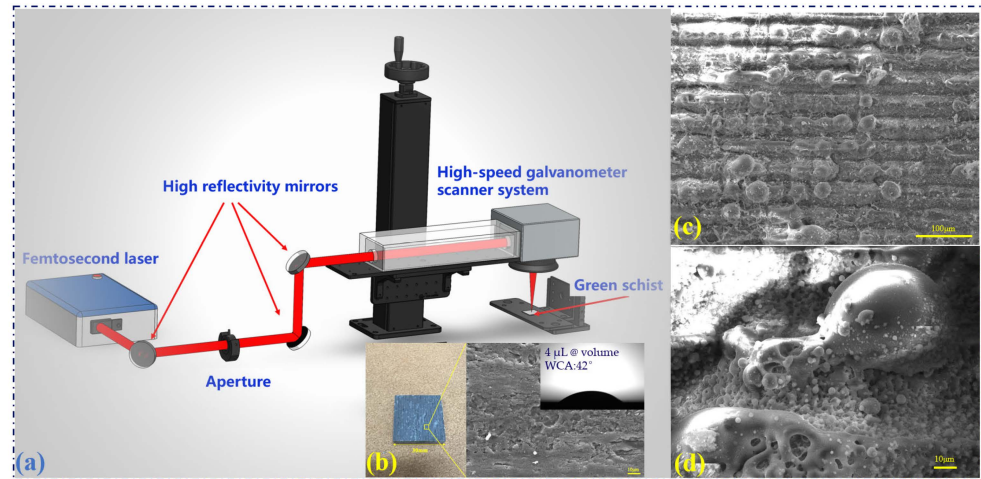


Figure 1. Femtosecond laser processing micro-nano structure for the green schist. (a) Femtosecond laser processing system. (b) Green schist and its surface microstructure. (c,d) Micro-nano structure processed by the femtosecond laser.

2.2. Experimental Setup

The stone components of ancient building complexes in Wudang Mountain are mostly in open or semi-open environments and usually exhibit surface flaking, with rain and high humidity being among the main causative environmental factors. Borrowing from the micro-nano superhydrophobic structure on the surface of lotus leaves, we consider processing a similar hydrophobic structure on the sample surface by femtosecond laser to achieve the purpose of conservation. The femtosecond laser (HR-Femto-IR-60, Huaray, Wuhan, China) used for processing the micro-nano textures on the green schist surface has a wavelength of 1035 nm, pulse duration of 238 fs ($M^2 \leq 1.3$). After passing through three total reflectors (reflectivity 99.6%@1035 nm), the laser beam with a diameter of 2 mm enters the two-axis high-speed galvanometer scanner system (14A1064, Zhibo-Tech, Shenzhen, China). The focused beam diameter on the green schist surface is calculated to be 33 μm by using a focus lens with a focused length of 80 mm [33]. A repetition rate of 100 kHz and a pulse energy of 40 μJ are used to process the sample (Figure 1a).

As a basis for laser processing textures on the green schist surface, we first tested the ablation morphology formed under the irradiating of the femtosecond laser with different pulse numbers to analyze the new phenomena that non-homogeneous samples may present. Based on this, we further explored the micro-nano structural features of the non-homogeneous samples and their corresponding hydrophobic properties by processing group holes and grooves on the sample surface. Figure 1c,d show the results of femtosecond laser processing. Repeated scanning by the femtosecond laser (10 times), while ablating the surface of the sample, the accumulation of localized heat caused the formation of molten parts.

2.3. Instruments and Characterization

The 3D morphology and surface profiles were investigated by a laser confocal microscope (Olympus, DSX1000, Tokyo, Japan). After the laser processing, a thin layer of silver particles was deposited on the surface by spraying before the subsequent sample analysis.

The morphologies of the sample surfaces were characterized using an MIRA3 LMU scanning electron microscope and backscattered electron microscopy (SEM and BSE, TESCAN, Brno, Czech Republic). Elemental analysis was performed by an energy-dispersive X-ray spectroscopy (EDS) installed in the SEM. The apparent water contact angle (WCA) was measured by an optical tensiometer (One Attension, Biolin Scientific, Espoo, Finland), whose built-in CCD camera can output the test images. The WCA results of samples were tested one day after laser processing. The volume of the water droplets tested was 4 μL .

3. Results and Discussion

3.1. The Ablation Performance of Femtosecond Laser to Green Schist

Small craters of varying depths are generally formed by the ablation of the femtosecond laser with different pulse numbers at the same pulse energy [34]. However, the ablation performance of the femtosecond laser to the green schist shows completely different results (Figure 2a). The number of femtosecond laser pulses irradiating on the sample surface increased from 500 to 40,000. Since the samples are typically non-homogeneous materials, the diameter and morphology of the craters are not related to the number of pulses, but rather to the different compositions in the ablation region. After we analyzed different ablation diameters and morphologies obtained by the femtosecond laser ablation, the processed green schist surface can be summarized into three typical ablation features (Figure 2b–d). As the regions marked with triangles in Figure 2a, the ablation morphology mainly shows craters (the diameter is about 35 μm) with high circularity and minimally heat-affected zones (Figure 2d). It is a typical cold processing feature of the femtosecond laser, where the ablated region exhibits very sharp edges. Among the three main components of green schist, quartz belongs to non-metallic materials. The absorption of the quartz to femtosecond laser is dominated by the nonlinear absorption, while the heat conduction effect is weak, and thus, its processing is mainly dominated by localized ablation [35]. Therefore, the regions marked by the triangles can be recognized as the ablated quartz material.

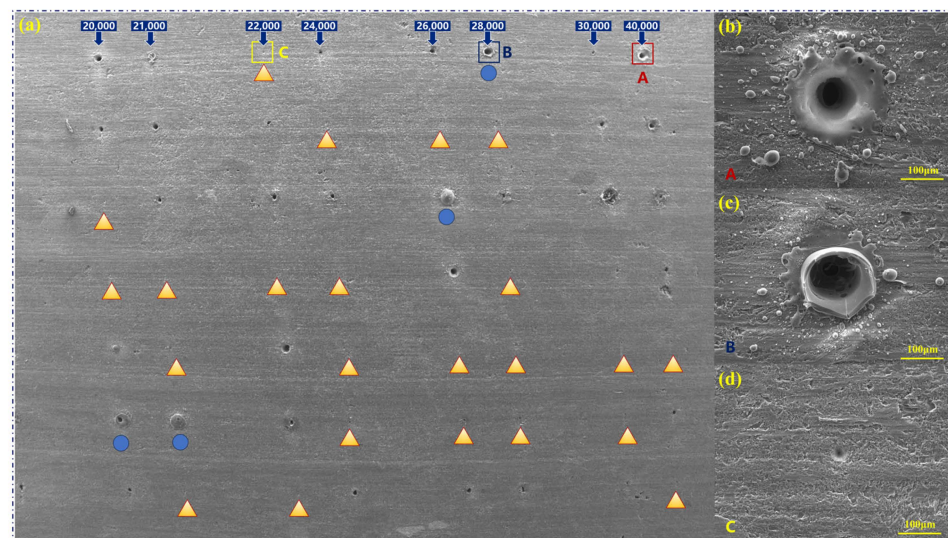


Figure 2. Femtosecond laser ablation of the green schist with 20,000–40,000 pulses. (a) Distribution of ablation craters, where the triangularly marked regions are the ablation results of the quartz, and the regions marked by circles are the ablation results of the muscovite (SEM image). (b) Ablation results of the chlorite. (c) Ablation results of the muscovite. (d) Ablation results of the quartz.

Another highly distributed ablation morphology shows the craters with a diameter of 100 μm and a high heat-affected zone (Figure 2d). Melted spheres of different diameters (hundred nanometers to 30 μm) recoiled on the sample surface and formed hierarchical micro-nano structures. Considering the composition and content of the green schist, the

morphology and quantitative distribution of this ablated region suggest that it is the result of femtosecond laser ablation of the chlorite composition. In fact, chlorite is rich in metallic elements, such as Fe and Mg, so the absorption to the femtosecond laser is dominated by linear absorption. Therefore, femtosecond laser ablation of chlorite reflects a high thermal effect under the irradiation of the 100 kHz femtosecond laser, and the chlorite is more easily removed by femtosecond laser ablation [36,37]. In addition, there are a few regions where the ablation morphology is dominated by the large thermal melting and thermal expansion, partly accompanied by ablated craters, typically as shown in Figure 2c. This is the morphology formed by the femtosecond laser ablation of the muscovite composition. In addition to containing a large amount of SiO_2 , muscovite also contains Al_2O_3 and K_2O . Under the irradiation of the femtosecond laser, some metal compounds can form effective absorption. The absorbed laser energy will have a heating effect on the SiO_2 through the heat conduction, eventually leading to localized expansion and ablation.

After elucidating the different ablation performances between different compositions of green schist to femtosecond laser, further processing of arrays of craters spaced $125\ \mu\text{m}$ apart in the aspect direction is achieved in the range of $6\ \text{mm} \times 6\ \text{mm}$. Meanwhile, to further distinguish the different morphologies of compositions under the femtosecond laser ablation, we further analyze the sample surface with a BSE image (Figure 3a). There is a clear color distinction between metallic compounds and non-metallic materials, and the quartz can be clearly distinguished from a variety of compositions, such as chlorite and muscovite. Also, the boundary between the femtosecond laser ablation region and the non-ablation region can be clearly defined in the figure (Figure 3a).

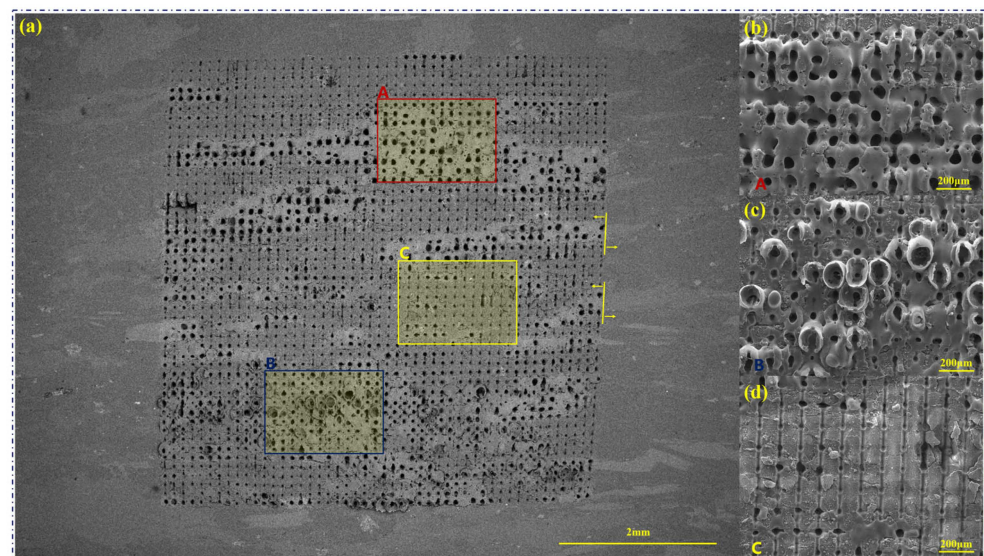


Figure 3. Femtosecond laser ablation of the green schist with 5000 pulses, which forms an array of craters spaced $125\ \mu\text{m}$ apart in the longitudinal and transverse directions. (a) Distribution of ablation craters (BSE figure). (b) Ablation results of the chlorite. (c) Ablation results of the muscovite. (d) Ablation results of the quartz.

Differences in ablation morphologies formed by the multiple compositions of the green schist are more pronounced in the case of the formation of crater arrays by femtosecond laser processing. Typical regions are shown, labeled A–C in Figure 3a. Region A is dominated by chlorite, and the melting phenomenon formed on the sample surface is more obvious under the high thermal effect, while the diameter of the craters formed by the ablation increases significantly (about $60\ \mu\text{m}$). Also, under the processing of the crater arrays, chlorite also embodies a higher thermal effect under the irradiation of the femtosecond laser, and a stable connection is formed between different ablation craters. As a result, the surface of the ablated region becomes smooth after heating and cooling, and there are no spherical

spatters appearing on the sample surface (Figure 3b). In addition, muscovite is usually distributed in the strips of chlorite, and we can also find a small amount of muscovite in the middle of chlorite in region B. The irradiation of the femtosecond laser causes the muscovite composition in this region to exhibit more pronounced thermal expansion, while the central region is ablated and impacted by the femtosecond laser to show cavities (Figure 3c) [38]. On the other hand, in Figure 3d, the quartz composition forms more stable craters under the femtosecond laser ablation. It is noticeable that part of the quartz contains a small amount of chlorite composition, and the melting of this part of the chlorite formed under the irradiation of the femtosecond laser is also more pronounced.

From the performance of the femtosecond laser single-point ablation of green schist described above, it is clear that the green schist, a material with complex compositions, especially as it contains some metallic and some non-metallic compounds, presents a significantly different response under the irradiation of the femtosecond laser. Trying to achieve a regular micro-nano structure by using the single-point ablation seems to be a challenge.

3.2. The Grooving Performance of Femtosecond Laser to Green Schist

Femtosecond laser processing of parallel grooves at a scanning speed of 60 mm/s is performed to further explore the performance of femtosecond laser processing method in grooving non-homogeneous green schist (Figure 4a). Due to the difference in electrical conductivity between the different compositions of green schist, multiple compositions, such as quartz and chlorite/muscovite, can also be distinguished under the SEM image of the processed groove. Among them, the quartz composition is less conductive, and this part is mainly dominated by a bright white color in the SEM image. The depth and width of the grooves formed are relatively small in the quartz composition due to its lower absorption to the femtosecond laser. Among the results obtained from the femtosecond laser grooving, we selected a region (region A) for analysis, as shown in Figure 4b–d. This region consists mainly of chlorite with some quartz (shown by the white box in Figure 4b) and muscovite (region C). The width of the grooves formed in the quartz composition is about 18 μm , the width formed in the chlorite composition is about 40 μm (Figure 4c), and the width formed in the muscovite composition is about 8 μm (Figure 4d).

The differences in laser absorption and thermal conductivity of the three compositions form a significant difference in the ablation, thermal melting, or thermal expansion characteristics, which are essentially the same as those under femtosecond laser single-point ablation. Among them, the ablation morphology of the chlorite composition is dominated by the cold ablation (Figure 4c), and the surface of the material after femtosecond laser processing shows a representative groove structure, with high stability [39]. Consequently, the femtosecond laser grooving of chlorite composition does not reflect the same high thermal effect as in Figures 2b and 3b. The high-speed scanning of the femtosecond laser is equivalent to about 500 femtosecond pulses irradiating at each position. It reduces the deposition of localized femtosecond laser energy compared with the femtosecond laser ablation with 5000 pulses, thus effectively controlling the thermal effect. On the other hand, the muscovite composition forms some melting under the high-speed scanning of the femtosecond laser, accompanied by smaller localized ablation (Figure 4c). Thus, the femtosecond laser grooving of muscovite composition is still dominated by typical thermal processing.

For a non-homogeneous material, such as green schist, measuring the surface elemental content and corresponding distribution after femtosecond laser grooving can accurately verify that the multiple types of morphologies correspond to which types of material compositions. We can focus on the EDS results of the regions not ablated by the femtosecond laser, which are almost unaffected by the femtosecond laser irradiation, in addition to being subjected to lower thermal conduction. The results of the elemental composition and content distribution of some of the grooved structures are shown in Figure 4e. Through the preliminary determination of SEM and BES images, as mentioned before, the main

composition of the selected region is chlorite, and a small amount of muscovite is included in the upper left corner of the region. In the EDS results, except for the labeled region (Figure 4e), the elements in the selected region are mainly dominated by O, Si, Mg, Al, and Fe, which is consistent with the main composition of chlorite and is also the same as the results of our determination through SEM and BSE images. In addition, the content and distribution of the multi-species elemental composition of chlorite in this region are stable, which is the reason why the formation of a stable groove structure can be observed in Figure 4a,b. The region marked in Figure 4e, which mainly contains the elements O, Si, Al, K, and Na, is consistent with the elemental species of the muscovite composition. The morphology of the region is also consistent with the thermal melting and expansion phenomena embodied in the muscovite composition under femtosecond laser ablation.

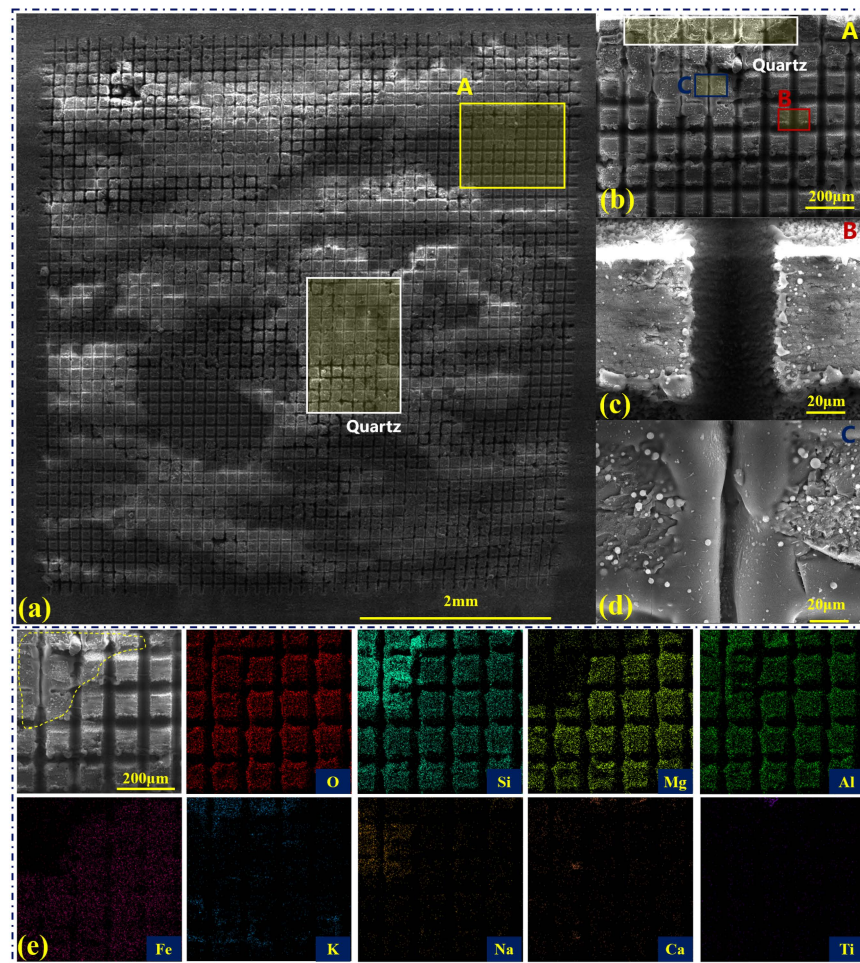


Figure 4. Results of the femtosecond laser grooving of the green schist, where the grooves are spaced at 125 μm in the aspect direction. (a) Characterization of the laser grooving. The reason the quartz component in the image looks to be at a different height than the other compositions is because of poor conductivity in that area, not a raised structure. (b) Localized enlargement in (a). (c,d) Localized enlargements in (b). (e) EDS and elemental mappings of the processed region.

In the processing of green schist by the high-speed scanning of the femtosecond laser, the scale of the grooves formed by different compositions varies, but the overall groove structure remains stable, which offers the possibility of realizing hydrophobicity. Among them, green schist has a high quartz content, and the processed quartz shows a limited groove depth and almost no micro-nano structures similar to those formed under the thermal accumulation (Figure 1c,d). In addition, the chlorite composition also reflects typical cold processing under femtosecond laser ablation. The processed region forms a

localized hierarchical micro-nano structure, but the overall depth is limited, and most of the region is still predominantly planar (Figure 4e). The muscovite composition forms a melt based on the single scan of the femtosecond laser and sputters some of the melt by the impact of the femtosecond laser ablation. Some regions form a micro-nano structure similar to the surface of the lotus leaf by depositing the melt [31]. However, the content of muscovite is only about 15%, which makes it difficult to play a decisive hydrophobic performance on the sample surface. The focus of the femtosecond laser grooving should thus be further on the quartz and chlorite compositions. For example, the thermal effect of the femtosecond laser ablation on the chlorite and quartz compositions should be increased by decreasing the scanning speed or increasing the scan numbers. After testing, we found that by lowering the scanning speed, e.g., to 10 mm/s, the femtosecond laser scanning strips off a certain thickness of material by the ablation and does not result in the formation of the desired three-dimensional micro-nano structure. Consequently, we adapt the approach of multiple scanning of the femtosecond laser to gradually enhance the thermal effect on the chlorite composition. At the same time, we also hope to form three-dimensional micro-nano structures in the quartz composition under the multiple ablations of the femtosecond laser.

The results obtained from 10 scans of the femtosecond laser are analyzed with SEM and BSE images (Figure 5a,b). Similar to the results in Figure 4, the quartz composition shows bright white under SEM image. Multiple scans and ablation of the quartz composition by the femtosecond laser gradually form a groove structure, and the ablated region forms a typical micro-nanostructure that resembles raised cones (Figure 5b). Since the Rayleigh length of the femtosecond laser after focusing is calculated to be 648 μm [33], the laser fluence can remain stable when the ablation depth is increased by multiple scans. At the same time, the processed region will be subjected to the impaction of the femtosecond laser-induced plasma shock wave, and then the ablation region will show a V-shaped structure under multiple scans [21]. As a result, the final structure on the sample surface resembles a cone, while the ablation and deposition over several scans create a typical micro-nano structure (Figure 5(b1)). In addition, part of the region forms heat accumulation under multiple scans, and the surface morphology is dominated by melting (Figure 5(b2)). The morphology of this melted region is close to that of the femtosecond laser ablation of the quartz composition, but it is more similar to the ablation results formed under the mixing of different compositions, which will be further explained by the analysis of the EDS results later. On the other hand, the morphology of the processed chlorite composition is dominated by protruding structures with a diameter of 20 μm because of the high absorption (labeled with white boxes, Figure 5a,c). In addition, the muscovite composition forms a more pronounced melting under multiple scans. Unlike the structure formed by a single scan (Figure 4d), all the processed muscovite composition in the region shows melting under multiple scans. It indicates that the high thermal effect and heat conduction of the muscovite compositions under femtosecond laser ablation causes the compositions in the non-processed region to reach the melting state as well.

Moreover, a region containing multiple compositions (region A) is used to analyze the surface elemental content and corresponding distribution. Partially separated quartz and chlorite are distinguished based on ablation morphology, brightness, and element distribution (labeled in Figure 5e). This region is a mixture of several compositions, with some regions containing high levels of the elements Mg, Fe, and K. By analyzing the elemental distribution of Si, we found that the composition in Figure 5e (labeled as yellow dashed line) is dominated by quartz but also contains some chlorite (elemental Al) and muscovite (elementals K and Na). It suggests that the green schist, a non-homogeneous material, especially the actual samples we obtained for use as stone components, which in addition to embodying independent distributions of multiple compositions, also has some regions that are a mixture of multiple compositions.

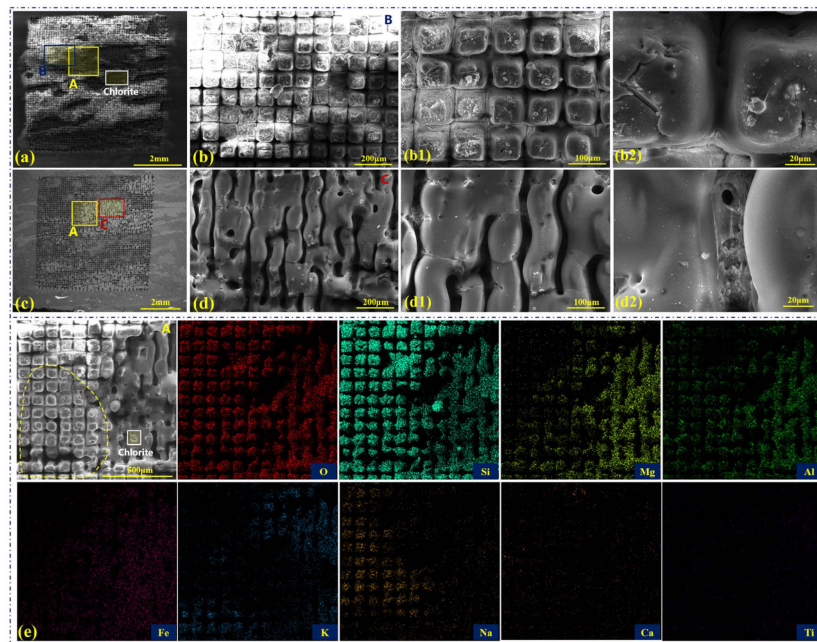


Figure 5. Results of the femtosecond laser grooving of the green schist, where 10 scans are adopted. (a) Characterization of the laser grooving (SEM image). (b) Localized enlargement in Figure 4a, where b1 and b2 are figures at different magnifications. (c) Overall distribution of laser grooving (BSE image). (d) Localized enlargement in Figure 4c, where d1 and d2 are figures at different magnifications. (e) EDS and elemental mappings of the processed region.

In general, although the compositions of green schist are complex, the overall grooving structures are relatively regular under the processing of single or multiple scans of the femtosecond laser. The ablation morphology of the three compositions, quartz, chlorite, and muscovite, can be taken as the typical features, and the ablation features of other regions containing multiple compositions will shift between these three typical ablation features. Both single-scan and multiple-scan femtosecond laser grooving results can obtain desirable micro-nano structures on the green schist surface. However, due to the difference between the high laser absorption of chlorite and muscovite compositions and the low laser absorption of quartz compositions, it is difficult for the femtosecond laser to homogeneously process the hydrophobic structures on the surface of green schist that is similar to the surface of lotus leaves.

3.3. Characterization of Surface Wettability after the Femtosecond Laser Grooving

In general, high roughness and low surface energy are the keys to obtaining super-hydrophobic surfaces [21]. For the modulation of the surface wettability of the stone components, one method is to keep the samples in air for a long time to obtain high hydrophobicity after processing the micro-nano structures [31], and the other is to add hydrophobic coatings on the surface [27]. After we process and characterize the femtosecond laser grooving samples with different groove spacing, we also further analyze the corresponding wettability. It can be observed that different compositions on the sample surface show different colors and morphologies after processing (Figure 6a), and the droplet can be retained on the sample surface with a large contact angle when measuring the wettability (Figure 6(a,a1)). This suggests that although the different compositions of green schist show different morphologies under femtosecond laser processing, including both macro and micro-nano structures, the sample surface can exhibit better hydrophobicity.

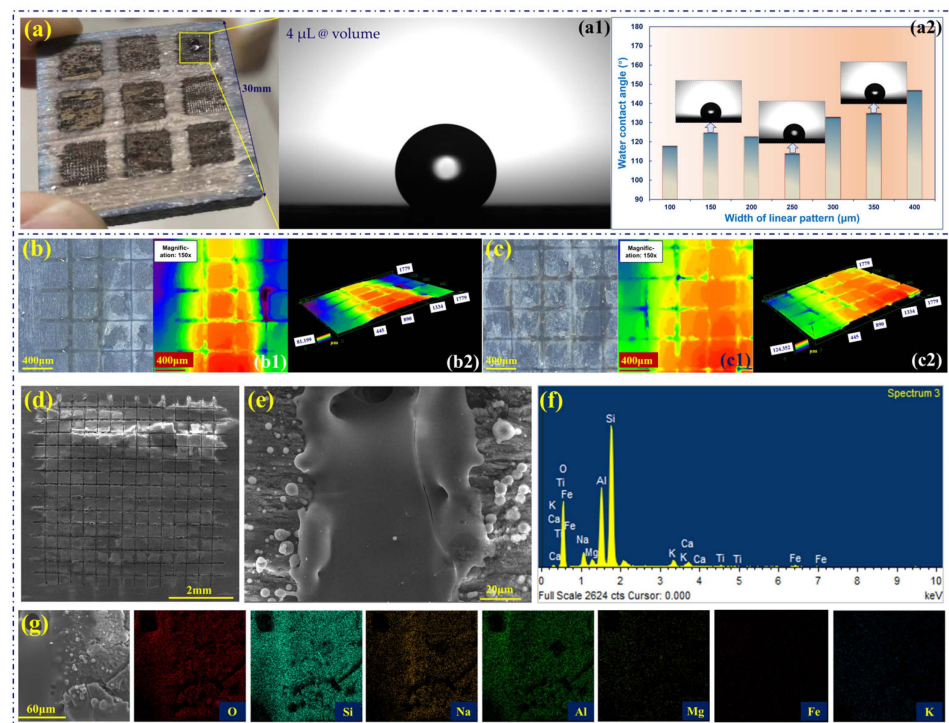


Figure 6. Wettability characterization and analysis after the femtosecond laser grooving. (a) The sample surface after processing by the femtosecond laser with different groove spacings, (a1) is the image of the water droplet on the green schist surface with a groove spacing of 400 μm , and (a2) is the result of water contact angles obtained with different groove spacings. (b,c) 3D morphology and surface profiles of the green schist surface with groove spacing of 400 μm , where (b) is the edge of the region, and (c) is the center of the region. (d) SEM image of the green schist surface with groove spacing of 400 μm . (e) SEM image of the chlorite composition processed by the femtosecond laser. (f,g) EDS and elemental mappings of the processed chlorite composition.

Contrary to our previous expectation, the maximum contact angles obtained after femtosecond laser processing of different groove spacings are not obtained when the spacing is minimum (100 μm in our experiments) but when the spacing is maximum (400 μm in our experiments, 147°), as shown in Figure 6(a1,a2). Considering the groove spacing of 400 μm , which is much larger compared to the femtosecond laser spot size of 30 μm , the sample surface is mostly dominated by non-ablated regions after the femtosecond laser processing. The 3D morphology and surface profiles of the processed sample are further analyzed, as shown in Figure 6b,c. Since the surface of the sample is obtained by SEDM with a line-cut spacing of 1.5 mm, the surface of the sample shows high and low undulations in the millimeter scale (Figure 6(b2,c2)). At the same time, the femtosecond laser processing region is dominated by grooves with a width of several tens of micrometers and a depth of about hundred micrometers (81.199 μm in Figure 6(b2) and 124.352 μm in Figure 6(c2)). In contrast, the non-femtosecond processed region is predominantly planar, with some regions deposited with sputtered spherical particles formed by the ablation of the femtosecond laser to the chlorite composition (Figure 6d,e, the chlorite composition can be determined from Figure 6f,g).

As a result, femtosecond laser processing at a groove spacing of 400 μm resulted in a few mm-hundred μm -few μm hierarchical structures. The large area of the non-processed region also ensured the stability of the distribution of this hierarchical micro-nano structure on the sample surface. The above mechanisms are believed to be the main reason for the high contact angle obtained on the chlorite surface after femtosecond laser processing of the 400 μm spaced grooves.

4. Conclusions

As an important cultural relic, the stone components of the ancient building complex in Wudang Mountain are of great value for its sustainable conservation significance. We take green schist, a typical multi-composition, non-homogeneous material as an example, and carry out a study on the mechanism and application of the femtosecond laser processing of the non-homogeneous material. The main conclusions are as follows.

- (1) The three compositions of green schist, quartz, chlorite, and muscovite show multiple types of performances under irradiation of the femtosecond laser. The nonlinear absorption of the femtosecond laser by the quartz composition reflects the cold ablation performance. The linear absorption of the chlorite composition reflects cold ablation (500 pulses) and melting (5000 pulses). The muscovite composition reflects typical thermal heating, melting, expansion, and ablation.
- (2) Due to the differences between the multiple compositions of green schist, the femtosecond laser single-point ablation does not result in the formation of a regular micro-nano structure on the sample surface. However, the scanning of the femtosecond laser can reduce the effect of compositional differences in the laser ablation performance, providing the possibility of high-performance laser processing of non-homogeneous material.
- (3) The multiple scanning of the femtosecond laser reduces the thermal effect of the femtosecond laser on the green schist and is thus suitable for the preparation of structures with varying groove spacing. In particular, the sample surface processed at a groove spacing of 400 μm obtains a high contact angle (147°), which is related to the formation of hierarchical micro-nano structures by the ablation of the femtosecond laser.

We believe that understanding the different structural characteristics of non-homogeneous materials formed by femtosecond laser processing, regulating the femtosecond laser parameters to obtain stable processing performance, and realizing a certain degree of hydrophobicity is expected to provide a completely novel method for the sustainable conservation of stone cultural relics. Later studies will further investigate the changes in hydrophobic properties of the sample surface under the action of air and rain over a long period of time (months, years, etc.). The laser shaping method will also be further explored to rectify the existing point spot into a line spot, thus improving the processing efficiency of the surface texture and facilitating the further development of related mobile and portable equipment.

Author Contributions: M.C. and C.W. (Chengaonan Wang): Conceptualization, validation, writing—original draft. K.L., X.J. and C.W. (Cong Wang): Discussion, writing—review and editing, funding acquisition. Y.W.: Conceptualization, validation, funding acquisition. All authors have read and agreed to the published version of the manuscript.

Funding: This research was funded by the National Natural Science Foundation of China (Grant No. 52278042 and 52105498).

Institutional Review Board Statement: Not applicable.

Informed Consent Statement: Not applicable.

Data Availability Statement: The data that support the findings of this study are available from the authors upon reasonable request.

Acknowledgments: We are very grateful to G. Zeng of the China University of Geosciences for his help in the identification of the different compositions and contents of the green schist. Also, we would like to thank the Wuhan Huaray Precision Laser Co., Ltd. for their support.

Conflicts of Interest: The authors declare no conflicts of interest.

References

1. Lei, Z.; Wan, L.; Zhang, Y. Investigation, Diagnosis, Assessment and Conservation Strategy for a Wall Painting at Wudang Mountain Taoist Temple Using BIM Technology. *Stud. Conserv.* **2018**, *63* (Suppl. S1), 377–380. [[CrossRef](#)]

2. Xu, W. Wild Edible Plants and Pilgrimage on Wudang Mountain. *J. Ethnobiol.* **2015**, *35*, 606–627.
3. Wang, C.; Chen, M.; Wang, Y. Surface flaking mechanism of stone components of ancient building complex in Wudang Mountain, China. *Constr. Build. Mater.* **2023**, *399*, 132611. [[CrossRef](#)]
4. Sadat-Shojai, M.; Ershad-Langroudi, A. Polymeric coatings for protection of historic monuments: Opportunities and challenges. *J. Appl. Polym. Sci.* **2010**, *112*, 2535–2551. [[CrossRef](#)]
5. Nosonovsky, M.; Bhushan, B. Biologically inspired surfaces: Broadening the scope of roughness. *Adv. Funct. Mater.* **2008**, *18*, 843–855. [[CrossRef](#)]
6. Weng, W.; Deng, Q.; Yang, P.; Yin, K. Femtosecond laser-chemical hybrid processing for achieving substrate-independent superhydrophobic surfaces. *J. Cent. South Univ.* **2024**, *31*, 1–10. [[CrossRef](#)]
7. Darmanin, T.; Guittard, F. Superhydrophobic and superoleophobic properties in nature. *Mater. Today* **2015**, *18*, 273–285. [[CrossRef](#)]
8. Lin, F.; Shuhong, L.; Yingshun, L.; Huanjun, L.; Lingjuan, Z.; Jin, Z.; Yanlin, S.; Biqian, L.; Lei, J.; Daoben, Z. Super-hydrophobic Surfaces: From Natural to Artificial. *Adv. Mater.* **2003**, *14*, 1857–1860.
9. Revez, M.J.; Raposo, M.; Rodrigues, J.D. The prodomea phasing and compatibility indicators as tools for the planning and design of conservation interventions. Assessment and validation in the santa clara-a-velha monastery (coimbra, portugal). In Proceedings of the International Congress on Deterioration & Conservation of Stone, New York, NY, USA, 22–26 October 2012.
10. Xu, S.; Wang, Q.; Wang, N.; Qu, L.; Song, Q. Study of corrosion property and mechanical strength of eco-friendly fabricated superhydrophobic concrete. *J. Clean. Prod.* **2021**, *323*, 129267. [[CrossRef](#)]
11. Wang, N.; Wang, Q.; Xu, S.; Lei, L. Green fabrication of mechanically stable superhydrophobic concrete with anti-corrosion property. *J. Clean. Prod.* **2021**, *312*, 127836. [[CrossRef](#)]
12. Liu, C.; Zheng, J.; Liu, X.; Yin, K.; Wang, H.; Wang, Q. Facile laser-based process of superwetting zirconia ceramic with adjustable adhesion for self-cleaning and lossless droplet transfer. *Appl. Surf. Sci.* **2023**, *638*, 158069. [[CrossRef](#)]
13. Yong, J.; Chen, F.; Li, M.; Yang, Q.; Fang, Y.; Huo, J.; Hou, X. Remarkably simple achievement of superhydrophobicity, superhydrophilicity, underwater superoleophobicity, underwater superoleophilicity, underwater superaerophobicity, and underwater superaerophilicity on femtosecond laser ablated PDMS surfaces. *J. Mater. Chem. A* **2017**, *5*, 25249–25257. [[CrossRef](#)]
14. Xu, J.; Su, Q.; Shan, D.; Guo, B. Sustainable micro-manufacturing of superhydrophobic surface on ultrafine-grained pure aluminum substrate combining micro-embossing and surface modification. *J. Clean. Prod.* **2019**, *232*, 705–712. [[CrossRef](#)]
15. Huang, X.; Sun, M.; Shi, X. Chemical vapor deposition of transparent superhydrophobic anti-icing coatings with tailored polymer nanoarray architecture. *Chem. Eng. J.* **2023**, *454*, 139981. [[CrossRef](#)]
16. Bai, X.; Yang, S.; Tan, C.; Jia, T.; Guo, L.; Song, W.; Jian, M.; Zhang, X.; Zhang, Z.; Wu, L.; et al. Synthesis of TiO₂ based superhydrophobic coatings for efficient anti-corrosion and self-cleaning on stone building surface. *J. Clean. Prod.* **2022**, *380*, 134975. [[CrossRef](#)]
17. Wang, J.; Zhang, Y.; He, Q. Durable and robust superhydrophobic fluororubber surface fabricated by template method with exceptional thermostability and mechanical stability. *Sep. Purif. Technol.* **2023**, *306*, 122423. [[CrossRef](#)]
18. Eryildiz, B.; Ozbey-Unal, B.; Menciloglu, Y.Z.; Keskinler, B.; Koyuncu, I. Development of robust superhydrophobic PFA/TMI/PVDF membrane by electrospinning/electrospraying techniques for air gap membrane distillation. *J. Appl. Polym. Sci.* **2023**, *140*, 53635. [[CrossRef](#)]
19. Yang, X.; Yang, N.; Gong, Z.; Peng, F.; Jiang, B.; Sun, Y.; Zhang, L. The superhydrophobic sponge decorated with Ni-Co double layered oxides with thiol modification for continuous oil/water separation. *Chin. J. Chem. Eng.* **2022**, *54*, 296–305. [[CrossRef](#)]
20. Zhao, J.; Gao, X.; Chen, S.; Lin, H.; Li, Z.; Lin, X. Hydrophobic or superhydrophobic modification of cement-based materials: A systematic review. *Compos. Part B Eng.* **2022**, *243*, 110104. [[CrossRef](#)]
21. Wang, C.; Ding, K.; Song, Y.; Jia, X.; Lin, N.; Duan, J.A. Femtosecond laser patterned superhydrophobic surface with anisotropic sliding for droplet manipulation. *Opt. Laser Technol.* **2024**, *168*, 109829. [[CrossRef](#)]
22. Zhang, C.; Zhang, X.; Shen, H.; Shuai, D.; Xiong, X.; Wang, Y.; Huang, H.; Li, Y. Superior self-cleaning surfaces via the synergy of superhydrophobicity and photocatalytic activity: Principles, synthesis, properties, and applications. *J. Clean. Prod.* **2023**, *428*, 139430. [[CrossRef](#)]
23. Schnell, G.; Polley, C.; Thomas, R.; Bartling, S.; Wagner, J.; Springer, A.; Seitz, H. How droplets move on laser-structured surfaces: Determination of droplet adhesion forces on nano- and microstructured surfaces. *J. Colloid Interface Sci.* **2022**, *630*, 951–964. [[CrossRef](#)]
24. Sun, X.; Fan, K.; Wang, Z.; Mei, R.; Yang, X. Regulation of hydrophobicity on yttria stabilized zirconia surface by femtosecond laser. *Ceram. Int.* **2021**, *47*, 9264–9272. [[CrossRef](#)]
25. Zhao, D.; Zhu, H.; Zhang, Z.; Xu, K.; Lei, W.; Gao, J.; Liu, Y. Transparent superhydrophobic glass prepared by laser-induced plasma-assisted ablation on the surface. *J. Mater. Sci.* **2022**, *57*, 15679–15689. [[CrossRef](#)]
26. Chantada, A.; Penide, J.; Riveiro, A.; del Val, J.; Quintero, F.; Meixus, M.; Soto, R.; Lusquiños, F.; Pou, J. Increasing the hydrophobicity degree of stonework by means of laser surface texturing: An application on Zimbabwe black granites. *Appl. Surf. Sci.* **2017**, *418*, 463–471. [[CrossRef](#)]
27. Carrascosa, L.A.M.; Zarzuela, R.; Botana-Galvín, M.; Botana, F.J.; Mosquera, M.J. Achieving superhydrophobic surfaces with tunable roughness on building materials via nanosecond laser texturing of silane/siloxane coatings. *J. Build. Eng.* **2022**, *58*, 104979. [[CrossRef](#)]

28. Ding, Y.; Liu, L.; Wang, C.; Li, C.; Lin, N.; Niu, S.; Han, Z.; Duan, J. Bioinspired Near-Full Transmittance MgF₂ Window for Infrared Detection in Extremely Complex Environments. *ACS Appl. Mater. Interfaces* **2023**, *15*, 30985–30997. [[CrossRef](#)]
29. López, A.J.; Pozo-Antonio, J.S.; Moreno, A.; Rivas, T.; Pereira, D.; Ramil, A. Femtosecond laser texturing as a tool to increase the hydrophobicity of ornamental stone: The influence of lithology and texture. *J. Build. Eng.* **2022**, *51*, 104176. [[CrossRef](#)]
30. López, A.J.; Ramil, A.; Pozo-Antonio, J.S.; Rivas, T.; Pereira, D. Ultrafast Laser Surface Texturing: A Sustainable Tool to Modify Wettability Properties of Marble. *Sustainability* **2019**, *11*, 4079. [[CrossRef](#)]
31. Ariza, R.; Alvarez-Alegria, M.; Costas, G.; Tribaldo, L.; Gonzalez-Elipe, A.R.; Siegel, J.; Solis, J. Multiscale ultrafast laser texturing of marble for reduced surface wetting. *Appl. Surf. Sci.* **2022**, *577*, 151850. [[CrossRef](#)]
32. Díaz, A.J.L.; Ramil, A.; Freire-Lista, D.M. Evaluation of femtosecond laser texturing on carbonate heritage stones. In *Lasers in the Conservation of Artworks XIII*; CRC Press: Boca Raton, FL, USA, 2023; pp. 234–244.
33. Jia, X.; Dong, J.; Wang, H.; Aleksei, K.; Zhu, G.; Zhu, X. High-speed drilling of alumina ceramic by sub-microsecond pulsed thin disk laser. *Opt. Express* **2020**, *28*, 33044–33052. [[CrossRef](#)]
34. Jia, X.; Luo, J.; Guo, C.; Li, Z.; Ma, Z.; Xiang, Y.; Yi, Z.; Li, K.; Wang, C.; Li, X.; et al. High-energy continuous wave laser ablation of alumina ceramic. *J. Mater. Res. Technol.* **2023**, *27*, 5389–5403. [[CrossRef](#)]
35. Xie, X.; Zhou, C.; Wei, X.; Hu, W.; Ren, Q. Laser machining of transparent brittle materials: From machining strategies to applications. *Opto-Electron. Adv.* **2019**, *2*, 18001701–18001713. [[CrossRef](#)]
36. Lin, Z.; Hong, M. Femtosecond Laser Precision Engineering: From Micron, Submicron, to Nanoscale. *Ultrafast Sci.* **2021**, *2021*, 9783514. [[CrossRef](#)]
37. Tan, D.; Zhang, B.; Qiu, J. Ultrafast Laser Direct Writing in Glass: Thermal Accumulation Engineering and Applications. *Laser Photonics Rev.* **2021**, *15*, 2000455. [[CrossRef](#)]
38. Pou-Álvarez, P.; Riveiro, A.; Nóvoa, X.R.; Fernández-Arias, M.; del Val, J.; Comesaña, R.; Boutinguiza, M.; Lusquiños, F.; Pou, J. Nanosecond, picosecond and femtosecond laser surface treatment of magnesium alloy: Role of pulse length. *Surf. Coat. Technol.* **2021**, *427*, 127802. [[CrossRef](#)]
39. Jia, X.; Chen, Y.; Liu, L.; Wang, C.; Duan, J. Advances in Laser Drilling of Structural Ceramics. *Nanomaterials* **2022**, *12*, 230. [[CrossRef](#)]

Disclaimer/Publisher’s Note: The statements, opinions and data contained in all publications are solely those of the individual author(s) and contributor(s) and not of MDPI and/or the editor(s). MDPI and/or the editor(s) disclaim responsibility for any injury to people or property resulting from any ideas, methods, instructions or products referred to in the content.